



DESY SUMMER STUDENT PROGRAMME 2018
REPORT

Towards Time-Resolved Raman Spectroscopy

at the monochromator beamline PG1
with RIXS endstation at FLASH

Student:	Amelie Marie Schulte
University:	Georg-August-Universität Göttingen
E-Mail:	a.schulte1@stud.uni-goettingen.de
Supervisors:	Günter Brenner, Siarhei Dziarzhytski
Group:	FS-FLASH-B
Duration:	17.07.2018 - 06.09.2018

Contents

1	Introduction	3
2	Theory	3
2.1	Resonant Inelastic X-Ray Scattering	3
2.2	Nickel Oxide	4
2.3	Time-Resolved Experiments	5
2.4	Nonlinear Optics	6
3	Experimental Setup	8
3.1	FLASH1 PG Monochromator Beamline	8
3.2	Raman Spectrometer	10
3.3	Optical Laser Setup	10
4	Project	12
5	Measurement Results	12
5.1	RIXS spectrum of NiO	12
5.2	Dispersion Measurements and Energy Calibration	13
5.3	Data Analysis	14
5.4	Build-Up Optical Laser Setup	17
6	Summary	18
	References	19

1 Introduction

The composition, behaviour and properties of materials were always an actual topic in many different regimes. In architecture, engineering and physics it is very important to know how the materials behave, especially to use the right materials for the right application. Different spectroscopy methods have led to a more detailed insight and understanding of the functionality of materials and the underlying fundamental physics processes involved. Resonant inelastic x-ray scattering (RIXS) gives a lot of information about the intrinsic excitations of certain materials and is the important examined process of Raman x-ray spectroscopy. In order to determine the electronic structure of materials spectrometers are often used. To learn something about the dynamical processes in the material, time-resolved RIXS measurements are getting more and more important. By using ultrabright femtosecond laser pulses with high photon energy in combination with a synchronized optical laser in a so called pump-probe scheme, different dynamical processes on the sub-picosecond time-scale can be investigated. Therefore, a pump-probe RIXS setup is built at the PG1 monochromator beamline as time-resolved RIXS spectroscopy endstation.

2 Theory

2.1 Resonant Inelastic X-Ray Scattering

Resonant inelastic x-ray scattering is an experimental technique that examines the inelastic scattered x-ray photons with a spectrometer. In the optical wavelength regime it is also often called resonant Raman spectroscopy. The incoming x-ray photons excite electrons from the core level into the empty valence band. The generated hole in the core state is then filled by an electron from the occupied valence band and a photon is emitted. Because of the interaction with the material the outgoing photon has less energy than the incoming photon [1]. The excitation of the electron to the unoccupied valence band has a momentum of $\hbar\vec{k}-\hbar\vec{k}'$ and energy of $\hbar\omega-\hbar\omega'$, whereby k and ω describe the incoming photon and k' and ω' the outgoing. This direct process is illustrated in

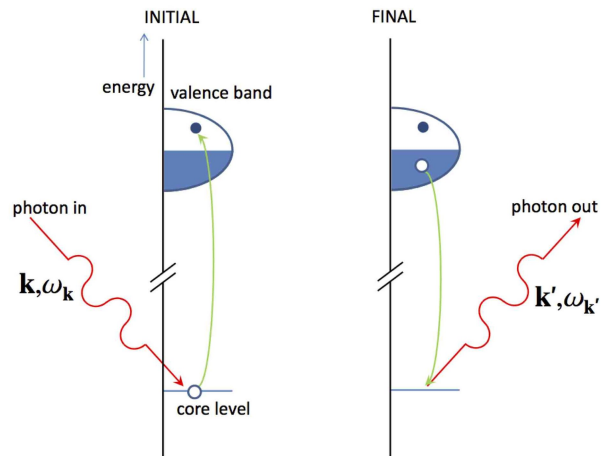


Figure 1: Direct RIXS process scheme: the incoming x-rays excite an electron to the valence band. The generated hole is filled by an electron of an occupied higher level, which leads to emission of a photon [1].

Figure 1. Also indirect processes with intermediate states can occur. The different energies of the outgoing photons can be observed with a spectrometer. By studying the energy loss of the photons, one can obtain information about the inelastic processes involved, e.g. charge transfer, d-d excitations, magnons or phonons. Different energies of the incoming photons excite different core electrons. The energy of the photon beam is chosen such that it resonates with one of the transitions of the system. High energy x-rays are used to excite at K and L absorption edges of the material, while soft x-rays and XUV photons mostly excite M edges. The scattering cross-section of the inelastic scattering can be very small compared to the elastic scattering. This implies that a high incident photon flux is required to measure the inelastic scattering, and therefore the intrinsic excitations. Resonances can enhance the inelastic scattering cross-section significantly, but the elastic scattering is always more probable [1].

Different excitations that can be measured with RIXS and their typical energies are shown in Fig. 2. Because of the width of the elastic line, phonon excitations are difficult to observe and require high-resolution spectrometers.

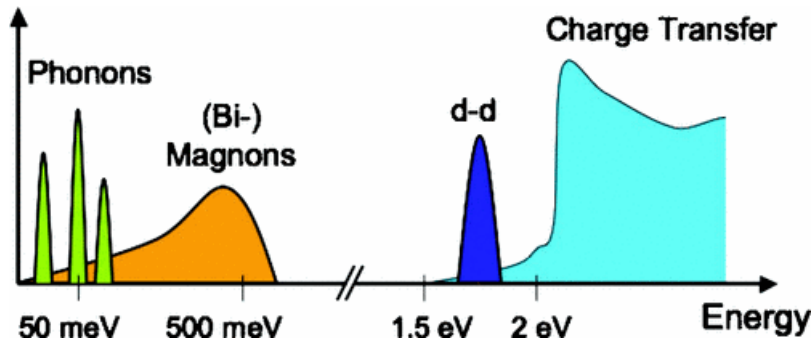


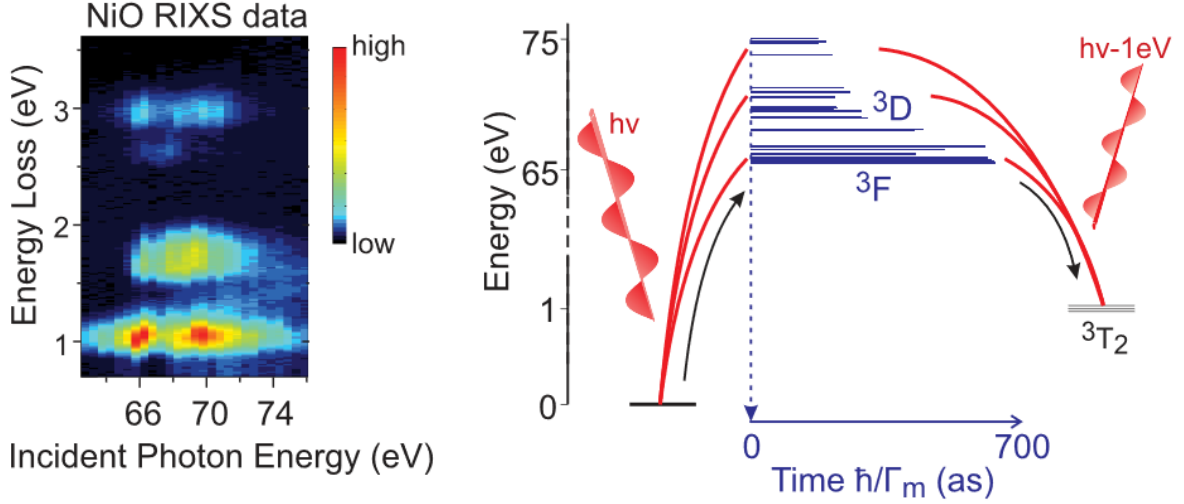
Figure 2: Different excitations like phonon excitations, d-d transitions or charge transfer that can be in principle measured with RIXS [1].

2.2 Nickel Oxide

NiO is a well characterized metal oxide. The Nickel atom is surrounded by ligands (oxygen atoms), whose field is not spherically symmetric. Thus, some d-orbitals attain higher energy levels (e_g) while other attain a lower energy level (t_{2g}) [2]. The orbital excitation from t_{2g} to e_g can be shown with inelastic scattering of high energy photons. Possible resonance pathways are shown in Fig. 3b). The blue bars represent transiently occupied intermediate states with different lifetimes (lengths of the bars).

XUV pulses can be used to excite the electrons from the t_{2g} into the e_g energy level, which has an energy difference of approx. 1 eV. Thus, the outgoing photons have 1 eV less energy than the incoming photons. This can be seen in the experimental measured data, compare Fig. 3a). Also signals with higher energy loss relating to excitations into

other levels could be observed. The strength of the signal depends on the chosen incident photon energy. Using resonance photon energies increase the efficiency of special transitions [2].



(a) NiO RIXS measurements with different incident photon energies. (b) Excitation of NiO orbitals with inelastic scattering using resonance frequencies.

Figure 3: NiO resonance pathways: electron excitation from t_{2g} to e_g , visible in the measured data with inelastic scattered photons who have an energy loss of 1 eV [2].

2.3 Time-Resolved Experiments

In order to perform time-resolved measurements, pump-probe schemes are often used. An optical laser pulse 'pumps' the sample, while the x-ray pulse 'probes' the current status of excitation in the material. By changing the delay between the two synchronized photon pulses using a delay stage, the dynamics of the sample can be investigated. A scheme of a typical pump-probe setup is shown in Fig. 4.

The direct RIXS process shown in Fig. 1 is happening really fast. By using ultrashort femtosecond laser pulses and scanning the time between excitation and relaxation, information like the rise and relaxation time can be observed. To pump the desired transition, resonance photon energies have to be used. Thus, different pump photon wavelengths are needed. This can be realized by nonlinear processes like harmonic generation with high intensity lasers. The basic theory is described in the following.

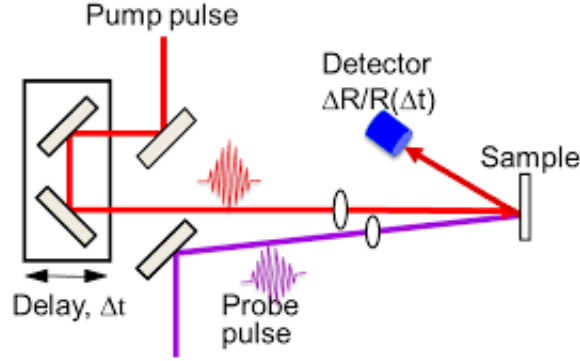


Figure 4: Time-resolved measurements using a pump-probe setup [3].

2.4 Nonlinear Optics

When low electromagnetic fields interact with matter, they generate a linear polarisation in the medium. This can be described by

$$P(\vec{r}, \omega) = \varepsilon_0 \cdot \chi^{(1)}(\omega) \cdot \vec{E}(\vec{r}, \omega). \quad (1)$$

Thereby ε_0 is the permittivity of free space and $\chi^{(1)}$ the linear susceptibility. By using ultrashort laser pulses, high pulse intensities are given. When these high electromagnetic fields interact with a material, the polarisation is not only linear depended on the field anymore:

$$P = \varepsilon_0 \left(\chi^{(1)} \vec{E} + \chi^{(2)} \vec{E} \vec{E} + \chi^{(3)} \vec{E} \vec{E} \vec{E} + \dots \right). \quad (2)$$

The nonlinear susceptibility $\chi^{(n)}$ is a n-dimensional tensor. Higher order nonlinear terms have now an effect on the polarization as well. Assuming an electric field of $\vec{E} = \vec{E}(t) \cdot \exp(i\omega t) + \vec{E}^*(t) \cdot \exp(-i\omega t)$, leads to a second order polarization $P_2 = \varepsilon_0 \chi^{(2)} \vec{E} \vec{E}$ with

$$\vec{E}^2(t) = E^2(t) \exp(2i\omega t) + 2E(t)E^*(t) + E^{*2}(t) \exp(-2i\omega t). \quad (3)$$

Thus, if light with high intensity travels through a medium with susceptibility χ^2 , light with double frequency (2ω) is created. This process is called second harmonic generation (SHG). The same happens for the third order, where terms with 3ω come up:

$$\begin{aligned} \vec{E}^3(t) = & 3E^2(t)E^*(t) \exp(i\omega t) + 3E(t)E^{*2}(t) \exp(-i\omega t) + \\ & + E^3(t) \exp(3i\omega t) + E^{*3}(t) \exp(-3i\omega t). \end{aligned} \quad (4)$$

Accordingly, this is called third harmonic generation (THG). It can be generated by sum-frequency generation (SFG), which is illustrated in Fig. 5. Two beams with different frequencies ω_1 and ω_2 travel through a nonlinear medium with χ^2 and create photons with new frequencies $\omega_3 = \omega_1 + \omega_2$ [4].

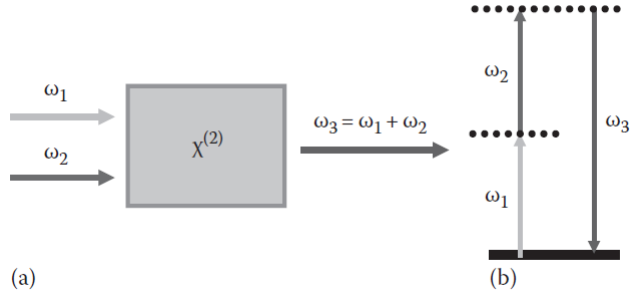


Figure 5: Sum-frequency generation scheme [4].

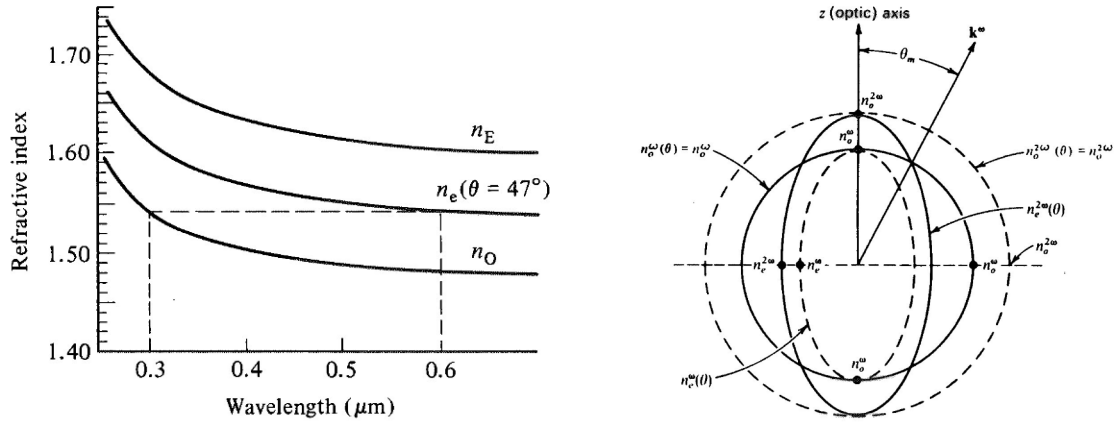
Phasematching

The highest photon intensity can be only reached if the beams interfere constructively. This is the case when the phase velocities are equal: $v_\omega = v_{q\omega}$, with q being the order of the harmonic. Because of the definition of the phase velocity $v = \omega/k$, the difference in wavevector is given by

$$\Delta\vec{k} = q \cdot \vec{k}_\omega - \vec{k}_{q\omega} = \frac{q\omega}{c}(n_{q\omega} - n_\omega), \quad (5)$$

which must be equal to zero for perfect phasematching. Because of dispersion, the existence of same refractive indices for both wavelengths is difficult. To realize this, a birefringent crystal can be used, since they have different refractive indices for different polarizations. The phasematching condition with $n_{2\omega} = n_\omega$ can be fulfilled for ordinary and extraordinary polarization. Depending on the crystal type, there can be found an angle relative to the optical axis for which the condition is valid. For positive birefringent crystals n_e is larger than n_o , so it must be $n_e^{(\omega)}(\theta_m) = n_o^{(2\omega)}$, whereby θ_m is the phasematching angle. For negative birefringent crystals, the condition is then $n_e^{(2\omega)}(\theta_m) = n_o^{(\omega)}$ [5]. An example of a positive birefringent crystal with phasematching angle of 47° is shown in Fig. 6a). The refractive index for extraordinary polarized light for a fundamental wavelength of 600 nm is equal to the refractive index of ordinary polarized light for the second harmonic (300 nm).

In Fig. 6b) the angle-dependence of the refractive indices for a negative birefringent crystal is shown. The phasematching angle has to be chosen such that the refractive indices are equal. In this scheme, it is the angle between the optical axis and the position where the one circle cross an ellipsoid.



(a) Refractive indices for a positive birefringent crystal: $n_{e,\omega}(\theta = 47^\circ) = n_{o,2\omega}$. (b) The phasematching angle is chosen such that the different refractive indices are equal for ω and 2ω .

Figure 6: Realization of phasematching condition $n_{2\omega} = n_\omega$ with a birefringent crystal [5].

Furthermore, the group velocity of a photon beam depends on the refractive index, which is wavelength dependent. Thus, the two beams travel with different group velocities and a group velocity mismatch (GVM) occurs. This means, that the two pulses (fundamental and second harmonic) have a time difference of $\Delta t = L \cdot \text{GVM} = L/v_g(\lambda/2) - L/v_g(\lambda)$. The parameter L is the length of the birefringent crystal and v_g the group velocity [6]. The effect is illustrated in Figure 7.

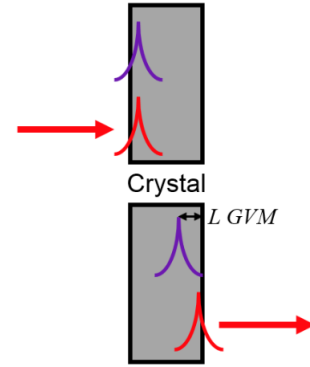


Figure 7: GVM [6].

3 Experimental Setup

3.1 FLASH 1 PG Monochromator Beamline

The RIXS experiments are performed at the PG1 monochromator beamline branch at the FLASH 1 facility. FLASH (Free-electron LASer Hamburg) is a soft x-ray free electron laser (FEL) which produces ultrashort pulses in the femtosecond regime. It consists of two undulator beamlines that can run at the same time: FLASH 1 and FLASH 2. The ultrashort x-ray pulses are generated by self-amplified spontaneous emission (SASE). In this process the accelerated electron bunches interact with the emitted photon beam in the undulator section, which in turn results in generation of coherent and high brilliant x-ray photon pulses. Since FLASH 1 uses so called fixed gap undulators the wavelength

of the photon pulses is purely determined by the electron beam energy, while at FLASH 2 variable gap undulators allow to tune the wavelength by changing the gap between the magnetic undulator structures. The electron bunch time pattern is directly imprinted onto the photon pulse time structure, resulting in photon pulses with 10 Hz repetition rate and up to 800 bunches in a 800 μs long bunch train. The separation of the pulses within the bunch train is 1 μs when running with 400 bunches. Possible photon energies at FLASH are between 20 eV-250 eV (fundamental) [7].

After the generation of the photon pulses, the electron beam is dumped, and the photon beam is guided to the PG1 beamline using grazing incident optics (see Fig. 8).

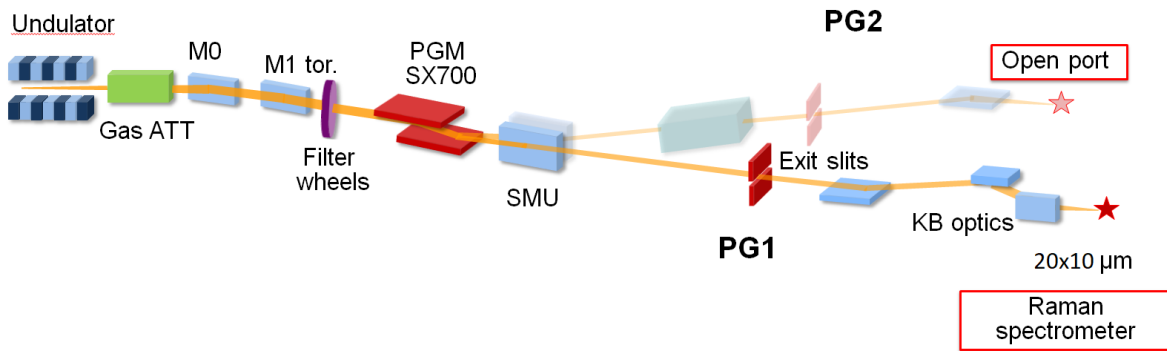


Figure 8: PG1 monochromator beamline at FLASH1 with PG2 in the background. The photon beam passes a plane grating monochromator (PGM) and is focused with KB optics on the sample. A focus size of $H \times V = 20 \times 10 \mu\text{m}$ FWHM can be reached in average (over many bunches).

Different photon diagnostics installed behind the undulator section allow to manipulate and characterize the photon pulses, e.g. measure intensity and beam position or attenuate the beam by means of a so called gas attenuator (Gas ATT). Following this section, the energy bandwidth of the FEL radiation - which is typically in the order of 1% can be reduced by using the plane grating (PG) monochromator beamline. A diffraction grating is used to energy disperse the FEL beam. By changing the angle, a different energy can be chosen. A mirror unit (SMU) allows to guide the beam either to the open port beamline PG2 or to the beamline branch PG1 with the Raman/RIXS spectrometer as permanent endstation. By changing the size of the exit slit, either a better resolution or more intense signals can be chosen. Kirkpatrick-Baez (KB) mirrors focus the XUV beam onto the sample in the UHV sample chamber (indicated by a star). The photon beam only travels in vacuum because of the high absorption of XUV in air.

3.2 Raman Spectrometer

Behind the sample chamber a double stage Raman spectrometer is mounted. Top and side view are shown in Figure 9. Currently, just the first stage is used in the following. It consists of two off-axis parabolic (OAP) mirrors and one diffraction grating. The focus point of the first mirror is located at the sample. After the first mirror, the beam is collimated and send on the grating. Depending on the experiment, different gratings with different groove density can be chosen for an energy range of 20-200eV. Behing the grating, the second OAP mirror focuses the beam onto the detector which is a in-vacuum CCD camera. It is located at the 'MS' position indicated in Fig. 9. To use the second stage of the spectrometer, a middle slit will be positioned there later and the detector at the end of the second spectrometer (SP2).

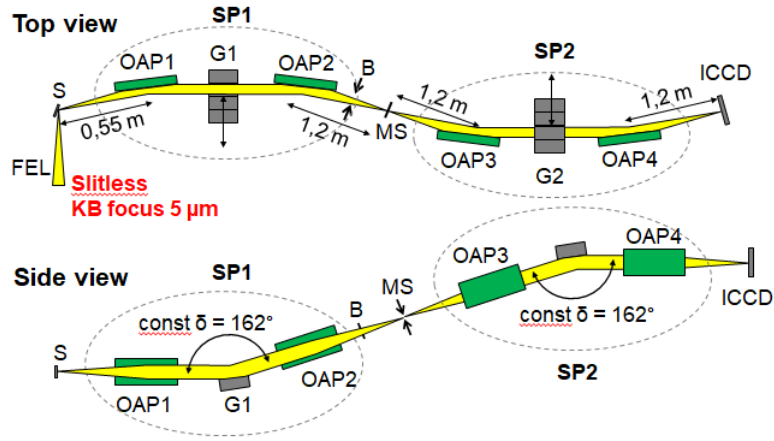


Figure 9: Top and side view of the two-stage Raman spectrometer. OAP1-4 indicate the off-axis parabolic mirrors while G is the diffraction grating. For the measurements within this summer student project only the first monochromator stage SP1 was used (see text).

3.3 Optical Laser Setup

In the FLASH 1 experimental hall, an optical laser with ultrashort pulses and synchronization to the FEL beam of FLASH is provided. It is an NIR beam with 800 nm wavelength, 13-17 μJ pulse energy and 90-100fs pulse length. Like the FEL, the laser has a repetition rate of 10Hz and the option to choose between 1 and 400 bunches. The pulse power at the end of the PG1 beamline (start of the optical setup) was measured to be 10 μJ per pulse. The planned optical setup for pump-probe RIXS experiments at the PG1 beamline branch is shown in Figure 10. The program Chi23D ([8]) was used to determine the required specifications and properties of the non-linear optics to obtain the desired results.

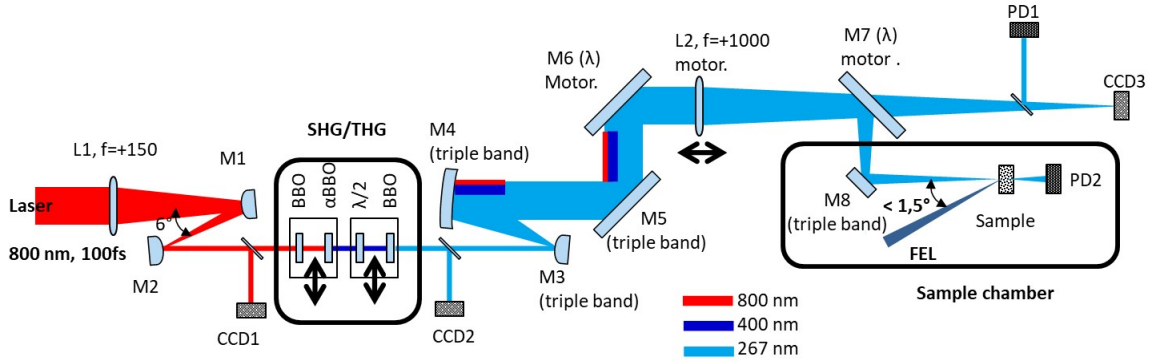


Figure 10: Planned optical setup for nearly collinear laser pump beam.

To have the possibility to pump the sample with different wavelengths, second and third harmonic are generated. As in chapter 2.4 described high intensities are needed for this nonlinear processes. Hence, compressing the beam size on a birefringent crystal would increase the conversion efficiency. Because of that, a lens focuses the beam and a telescope collimate it again. For that purpose two plano-convex mirrors with high reflectivity at 800 nm are used. A beta Barium borate (BBO) crystal is used for SHG, thus generating a 400 nm beam. Because of the group velocity mismatch (GVM), the pulses of the fundamental (800 nm) and the second harmonic (400 nm) exhibit a time difference after the conversion process. To compensate this time delay, an alpha BBO is used. It generates the opposite GVM, so that the pulses can again travel simultaneously and reach the THG crystal at the same time. After the α -BBO, a waveplate is mounted. It acts like a $\lambda/2$ -plate for 800 nm and λ -plate for 400 nm. Thus, the initially horizontal polarized 800 nm beam is going to be vertical polarized. The polarization of the 400 nm beam is rotated by 180° , so still vertical. Hence, both beams are then vertical polarized, which is required for the generation of the third harmonic. With the right polarization, the fundamental beam and the second harmonic pass the second BBO and generate the third harmonic by sum-frequency-generation. To adjust the phasematching angle, all crystals are mounted on rotatable mirror holders. Moreover, they are positioned on a movable stage, so they can be removed. This enables the possibility to chose between fundamental, second harmonic or third harmonic as pump laser. Before and after this frequency conversion stage, CCD cameras are placed to get information about the beam shape. The optimal settings are saved and used as reference for adjusting for next measurements. Afterwards, the beam is enlarged again by a second telescope. The focusing of a larger beam enables smaller focus sizes on the sample. For the second telescope triple-band mirrors are used. They have high reflection coefficients for all three wavelengths. The following mirrors M6 and M7 are only for one wavelength high reflective. Thus, the desired wavelength for the experiment has to be chosen in advance and the associated mirrors have to be mounted. A lens, which can be moved along the

optical axis for adjusting for the right wavelength, focuses the chosen beam onto the sample. The last mirror (M8) is mounted inside the ultra-high vacuum sample chamber, which is used to guide the laser beam as collinear as possible to the FEL beam towards the sample.

4 Project

During the summer student program, the author participated at FEL beamtimes, where RIXS spectra of NiO have been acquired. The measured data were edited and analyzed. This serves knowledge about the given resolution of the RIXS spectrometer and the possible measurable dynamic range. By changing the photon beam energy with the primary monochromator, the dispersion of the spectrometer at the detector could be measured and an energy calibration has been done as well. A reference spectrum of NiO for future time-resolved measurements was measured, analyzed and compared to already existing data from synchrotron measurements.

Besides the data analysis of the recorded NiO RIXS spectra, a second major activity was the realization/implementation of the optical setup for time-resolved RIXS at FLASH (see Chapter 3.3). The experimental setup was built, aligned and the SHG/THG frequency conversion was first achieved and then optimized.

5 Measurement Results

5.1 RIXS spectrum of NiO

A NiO sample was analyzed with the Raman spectrometer by using an FEL energy of 70.5 eV and 180 bunches. The elastic line and RIXS spectra were measured separately and stitched together at the end. The raw image of the RIXS signal without background subtraction is shown in Fig. 11.

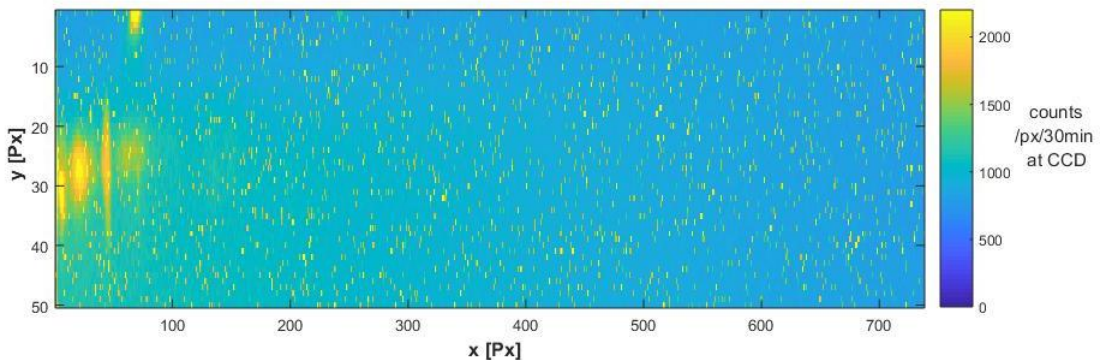


Figure 11: Measured RIXS signal, whereby the elastic line is shifted to the side such it is not detectable by the chip anymore. An acquisition time of 30 minutes was used.

To measure the RIXS signal, a longer acquisition time was used and the elastic line was shifted out of the measurement area to the left (negative x-pixels). The RIXS signal should be parallel to the camera bins to analyze it properly. Therefore, the picture is rotated by 4 degrees. A region of interest (ROI) ([yrange,xrange]=[15:40,1:250]) is chosen to concentrate on the signal area. The processed image is shown in Fig. 12.

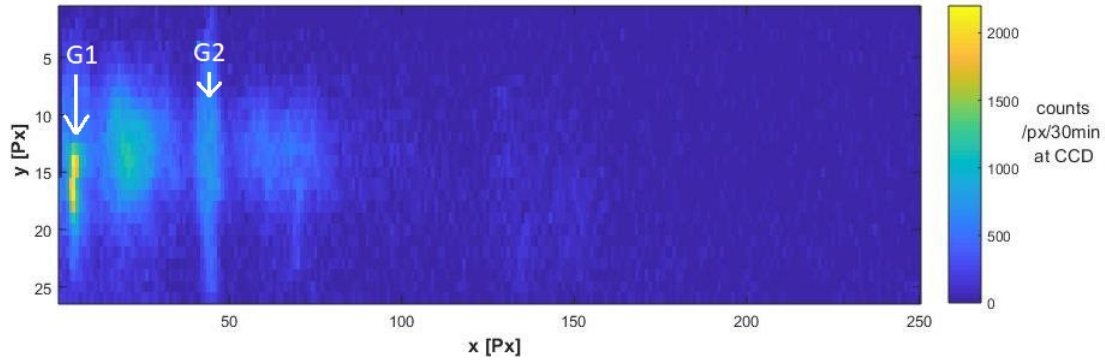


Figure 12: Region of interest (ROI) of RIXS signal, which was rotated. Additionally to the signal ghost peaks from the diffraction grating could be observed. They are indicated in the Figure as G1 and G2, see the text below for more information.

5.2 Dispersion Measurements and Energy Calibration

To measure the dispersion on the detector, the energy of the elastic line was changed by the monochromator and the pixel-position was observed. The data is shown in Fig. 13.

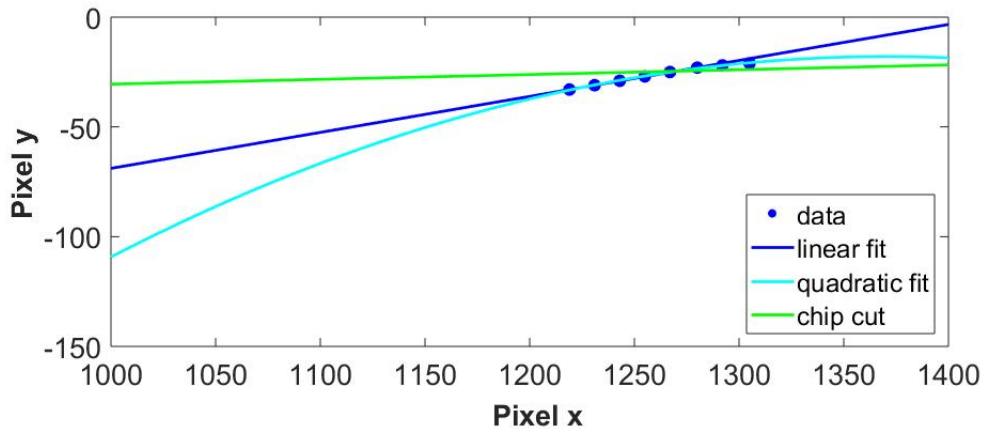


Figure 13: Dispersion measurements: change in energy of the elastic line from 70.5 eV to 69.1 eV in 0.2 eV steps shows a linear slope, which leads to a dispersion of 16.3 meV per pixel.

The energy was chosen from 70.5 eV till 69.1 eV and changed in 0.2 eV steps. As one can see, the central position of the signal leads to a linear graph, except the last two peaks ($E=69.3$ eV and $E=69.1$ eV), which are not on this line. Because of that a quadratic fit was also tested. But the observation of the position of the chip showed that the signals could not be observed properly. There is an artefact of the camera, namely the chip did not detect photons above certain pixels. The boundary, over which nothing can be detected is fitted in Fig. 13 as well (green line). Consequently, some part of the signal must have been cut and hence, the center of the seen signal is not the real one. Because of that, they were not taken into account any longer and the linear regression led to a dispersion of 16.3 meV per pixel.

Calibrating the x-axis of the measured data to an energy axis can now be done by using this dispersion measurement and the knowledge of the amount of shifting of the elastic line out of the picture. In Figure 14 the data of the RIXS signal is summed up over all 26 pixel (ROI in y-direction) and plotted against this calculated energy.

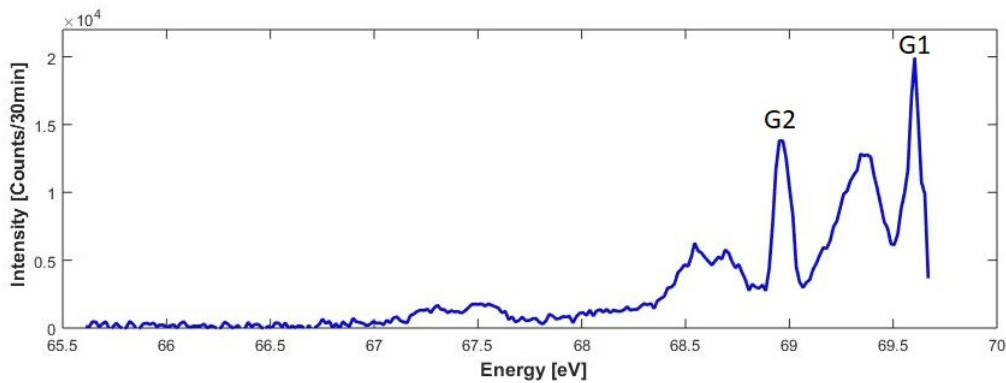


Figure 14: Integrated and background subtracted data of RIXS signal plotted with energy calibrated x-axis. Ghost peaks appear at 69.6 eV and 69 eV and are equally indicated as in Fig. 12.

The two tall peaks at approx. 69.6 eV and 69 eV are artefacts from the diffraction grating due to ruling errors. They can be seen on the higher and lower energy side of the elastic line.

5.3 Data Analysis

Because of such a different scattering cross-section of the elastic scattering and the inelastic scattering, the elastic line which has a photon energy of 70.5 eV were measured separately. As mentioned in chapter 2.1, much longer acquisition times are needed to measure the RIXS signal, but just one second is enough to have a proper signal of the elastic line. Thus, the elastic line was measured within an acquisition time of 1 s and this measured raw image without background subtraction is shown in Fig. 15.

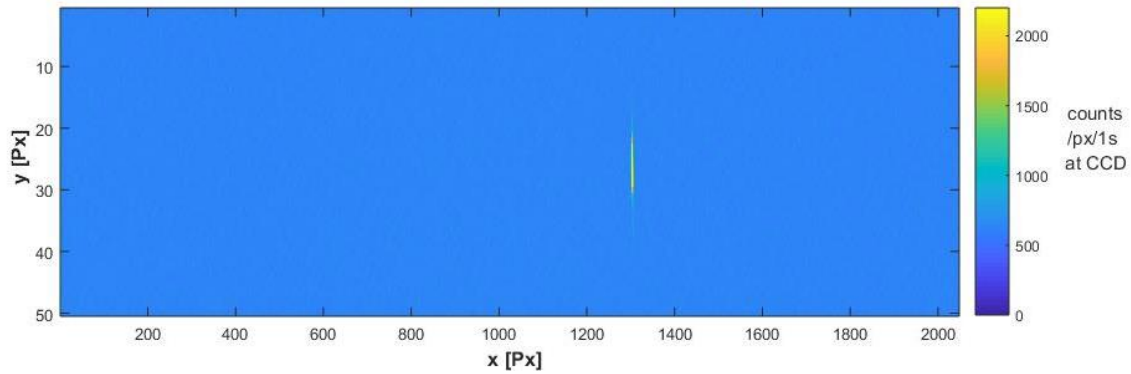


Figure 15: Measured elastic line with 1 s acquisition time.

To have a good overview, the image of the elastic line is also integrated, calibrated and stitched to the data of the inelastic scattered light. The two artefacts mentioned above are fitted with Lorentz-curves and subtracted from the data. The result is shown in Fig. 16. Measuring the FWHM of the elastic line by fitting the data with a Gaussian distribution leads to a value of 50.8 meV, which can also be seen in Fig. 16. This defines the resolution of the spectrometer.

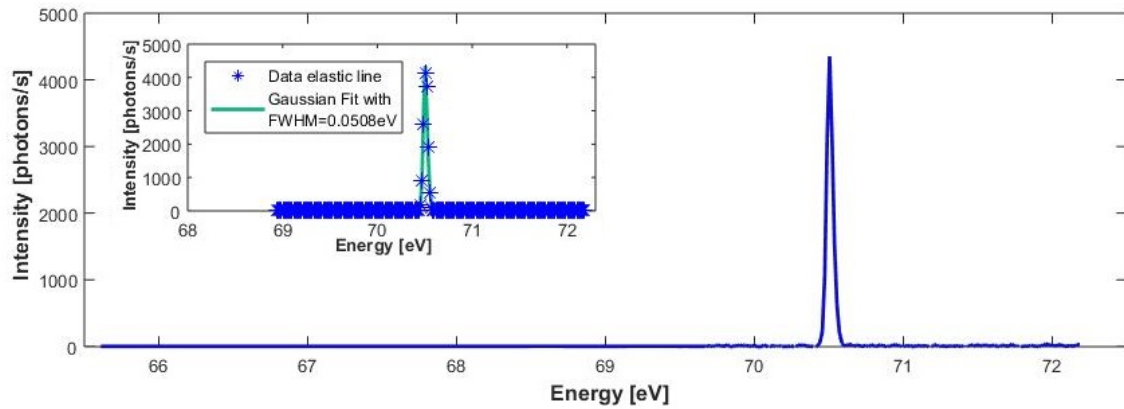


Figure 16: NiO spectrum with elastic line at 70.5 eV and RIXS signal with very low intensity at lower energies. The two measurements from above are stitched together, so from 69.67 eV on the other measurement begins. This can be seen in the different noise level as well. Moreover, the elastic line was fitted to determine the FWHM, which is 50.8 meV (see inset).

As mentioned in chapter 2.1, the intensity of the elastic line is much higher because of a higher scattering cross-section. To see the RIXS signal, a zoomed image is illustrated in Fig. 17.

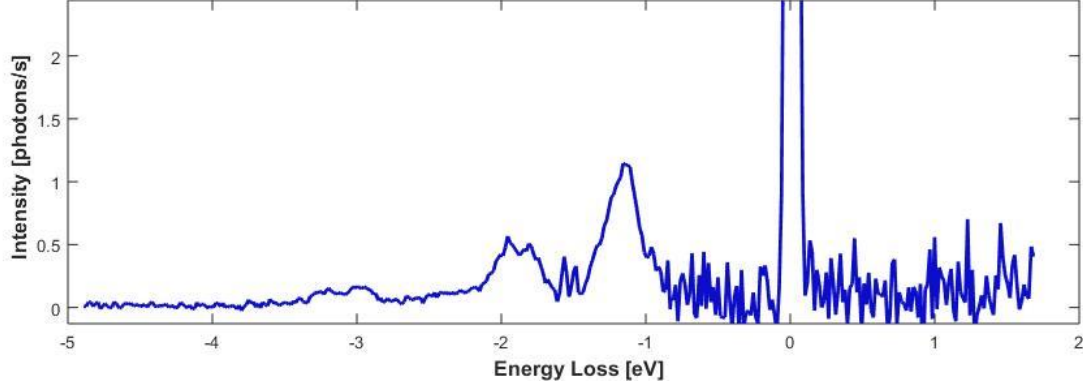


Figure 17: Zoom into RIXS signal in spectrum of Fig. 16. The elastic line at 0 eV energy loss has much higher intensity than the inelastic scattered signal, which could be still observed by using a longer acquisition time of 30 minutes.

The x-axis is changed to energy loss, which refers to the energy loss between incoming and outgoing photon. Next to the elastic line at 0 eV loss, three signals at ≈ -1.15 eV, -2 eV and -3 eV are detected. These signals were measured before (compare Fig. 3 in chapter 2.2) and Fig. 18 on the right, where the RIXS spectrum of NiO at the M absorption edge was measured with synchrotron radiation [9]. All measurements could obtain the same signals at approximately -1 eV, -2 eV and -3 eV, which indicate the d-d excitations from t_{2g} to the e_g level. Therefore, the expected and in literature described signals could be observed, which leads to the assumption that the measured spectrum is a good reference for further time-resolved measurements.

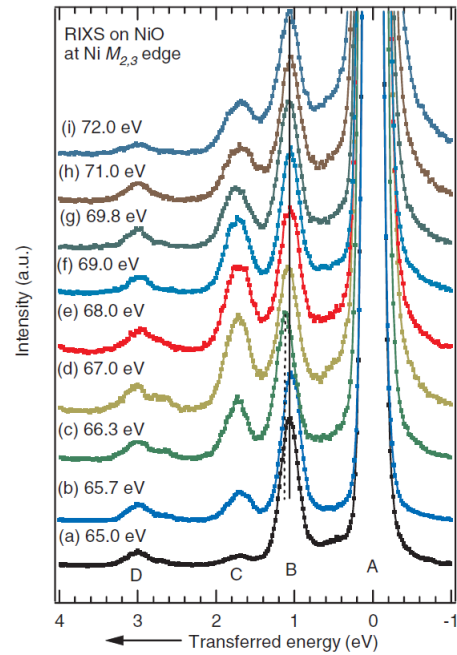
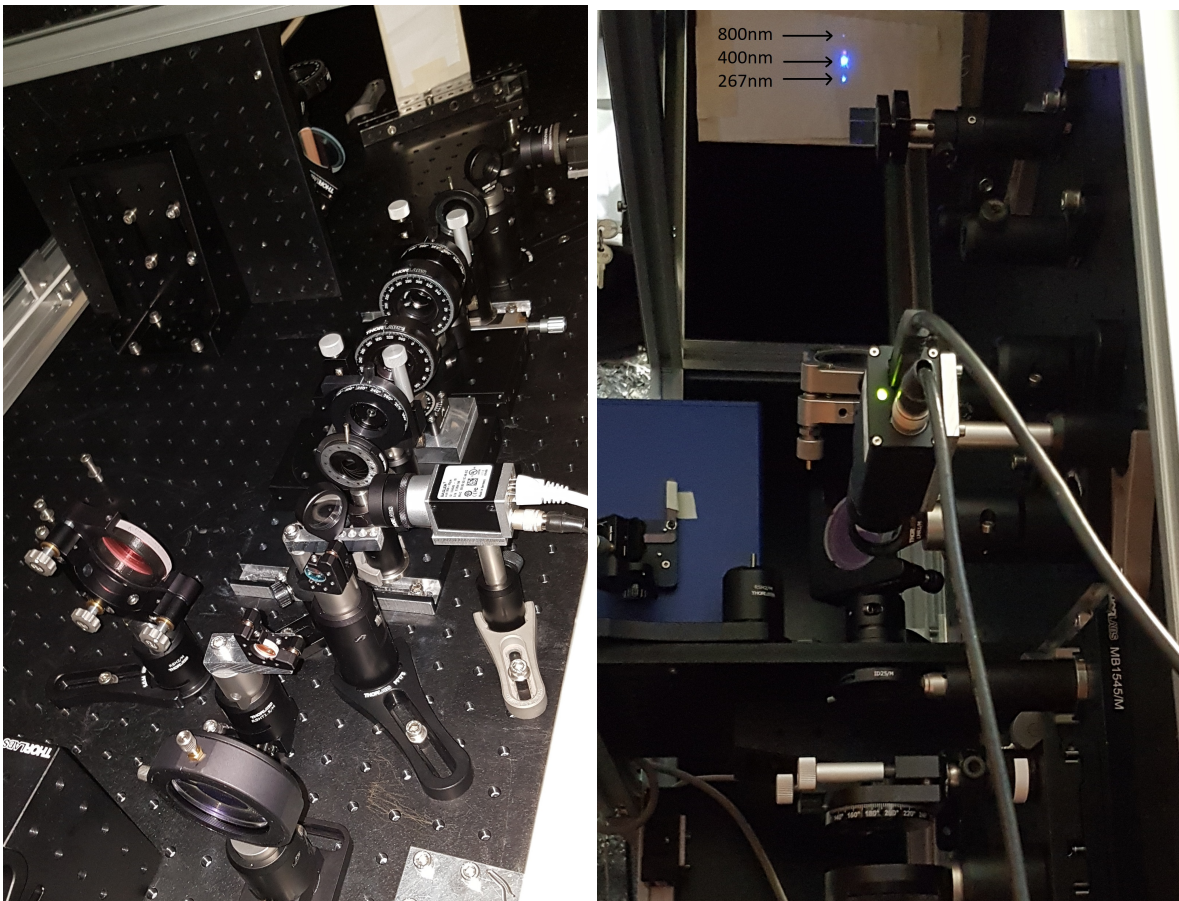


Figure 18: Measured RIXS signal of NiO using synchrotron radiation [9].

5.4 Build-Up Optical Laser Setup

Because of limited space in the experimental hall, the setup was built vertical. A part of the setup described in chapter 3.3 including the frequency conversion is shown in Fig. 19a). After the movable frequency conversion stage, a prism is mounted, which splits the three beams up. The different beams can be seen on a screen, see Fig. 19b). With this method, the frequency conversion could be optimized. By using a powermeter the intensity could be measured. The fundamental, the second harmonic and the third harmonic had a power of $10\ \mu\text{J}/\text{pulse}$, $1\ \mu\text{J}/\text{pulse}$ and $0.07\ \mu\text{J}/\text{pulse}$, respectively. In the future, the sample chamber will be opened and the last mirrors mounted. The pulses will be characterized with an autocorrelator and optimized by compressor adjustments in the laser hutch.



(a) Setup with frequency conversion stage

(b) Generation of second harmonic and third harmonic visible on the screen

Figure 19: Vertical setup for the optical laser beam for pump-probe experiments.

6 Summary

During the DESY Summer Student Programme the way to time-resolved RIXS experiments at FLASH were brought forwards. During a beamtime with the free electron laser FLASH a reference spectrum of NiO could be measured and analyzed. This good resolved spectrum can be used for future time-resolved experiments. To perform these, the FEL beam and an optical laser which is synchronized with the FEL will be used as probe and pump pulses, respectively. For different pump-pulse energies, a frequency conversion stage was built and optimized. Thus, pump pulses with energies of 800, 400 and 267 nm can be used in the future for pump-probe experiments.

References

- [1] Ament, Luuk J. P. et al., *Resonant inelastic x-ray scattering studies of elementary excitations*, Reviews of Modern Physics, Volume 83, No. 2, 705 (June 2011).
- [2] Wray, L.A. et al., *Extending resonant inelastic X-ray scattering to the extreme ultraviolet.*, Frontiers in Physics, Volume 3, Article 32 (May 2015). doi: 10.3389/fphy.2015.00032
- [3] Angle-resolved Photoemission and ultrafast Dynamics, Zhou Lab, Department of Physics, Tsinghua University, http://info.phys.tsinghua.edu.cn/zhou/ZhouLab_Research_Ultrafast\%20time-resolved\%20optical\%20pump-probe\%20technique.html, last visit: 30.08.2018
- [4] CRC, edited by Tupei Chen, Yang Liu, *Semiconductor Nanocrystals and Metal Nanoparticles: Physical Properties and Devices*, Edition: 1ST, 2016, Chapter: 9, pp.307-341
- [5] Diels, Jean-Claude and Rudolph, Wolfgang, *Ultrashort laser pulse phenomena: fundamentals, techniques, and applications on a femtosecond time scale*, 2. edition, Amsterdam a.o., Acad. Press/Elsevier, 2006
- [6] Trebino, Rick; *Ultrafast Optics Group - English Lectures*, 2016-2017, <http://frog.gatech.edu/talks.html>, last visit: 31.08.2018
- [7] Martins, M. et al., *Monochromator beamline for FLASH*, Review of Scientific Instruments 77, 115108 (2006); doi: 10.1063/1.2364148
- [8] Chi2D and Chi3D, program to simulate the frequency conversion processes between femtoscond laser pulses in birefringent nonlinear crystals, chi23d.com, last visit: 30.08.2018
- [9] Chiuzbăian, S.G. et al., *Localized Electronic Excitations in NiO Studied with Resonant Inelastic X-Ray Scattering at the Ni M Threshold: Evidence of Spin Flip*, Phys. Rev. Lett. 95, 197402, Published 31 October 2005